

SUSY Signatures at LHC

Frank E. Paige

Brookhaven National Laboratory, Upton, NY 11973 USA

Abstract

The ATLAS and CMS Collaborations at the CERN Large Hadron Collider (LHC) have devoted considerable effort to the study of SUSY signatures and measurements. This talk provides an overview of what can be learned at the LHC if TeV-scale SUSY exists.

1 Introduction

SUSY is perhaps the most promising candidate for physics beyond the Standard Model; it also provides a good test of detector performance. The ATLAS [1] and CMS [2] Collaborations at the CERN Large Hadron Collider (LHC) have therefore devoted a lot of effort to studying SUSY signatures and measurements. This talk provides an overview of that work with emphasis on new results since the overviews in Ref. 3 and 4.

The SUSY cross section at the LHC is dominated by the associated strong production of gluinos and squarks. If R parity is conserved, these decay into the lightest SUSY particle $\tilde{\chi}_1^0$, which escapes the detector, plus quarks, gluons, and perhaps other Standard Model particles. Thus, SUSY provides signatures containing at least jets and large missing transverse energy \cancel{E}_T . The LHC should be able to observe these signals for \tilde{g} and \tilde{q} masses up to about 2 TeV with only 10 fb^{-1} of integrated luminosity.

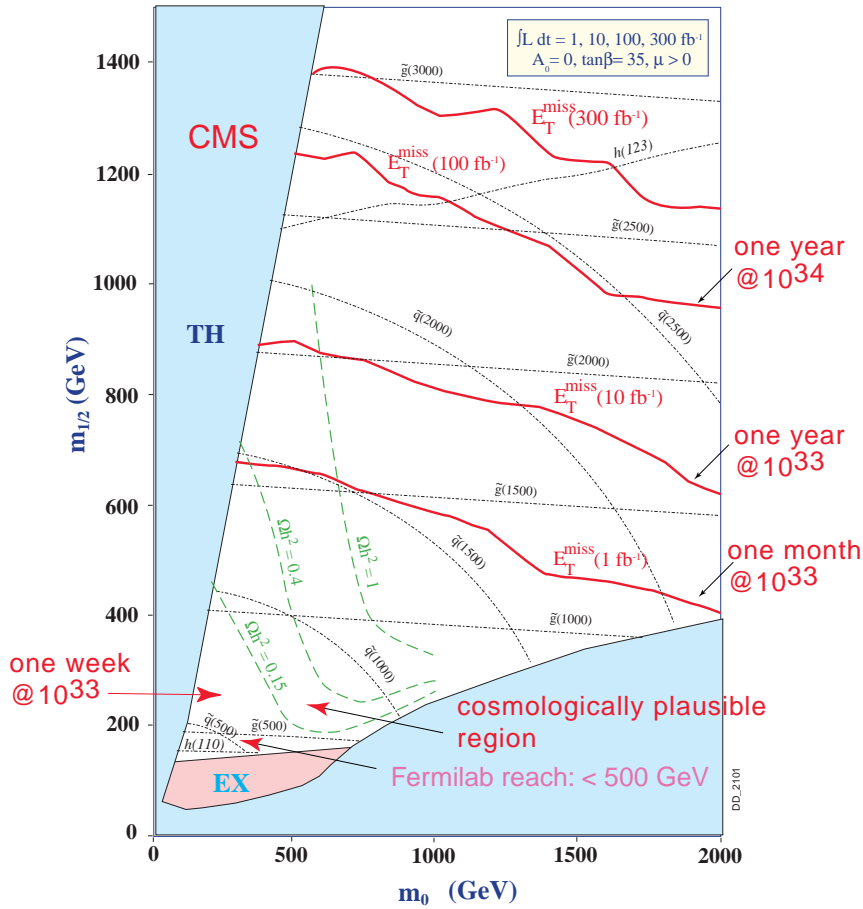
The challenge at the LHC is not to discover TeV-scale SUSY (assuming it exists) but to make precision measurements of masses and other quantities. Since the decay products of each SUSY particle contain an invisible $\tilde{\chi}_1^0$, no mass peaks can be reconstructed directly. Instead, masses must be inferred [5] from kinematic endpoints and other properties of the events. Developing methods to do this has been a main emphasis of the studies to date. Typically, events are simulated for a particular SUSY model and for the Standard Model backgrounds using a parton shower Monte Carlo program such as HERWIG [6], ISAJET [7], or PYTHIA [8], the detector response is simulated using a fast parameterization, cuts are made to give a good signal/background, and various kinematic distributions are reconstructed. A number of examples are presented below.

2 Search for SUSY

Since \tilde{g} and \tilde{q} are strongly produced, their cross sections are comparable to QCD at the same Q^2 . If R parity is conserved, their decays produce distinctive events with large \cancel{E}_T . A typical analysis requires at least four jets with $E_T > 100, 50, 50, 50 \text{ GeV}$ and $\cancel{E}_T > 100 \text{ GeV}$ and plots as a measure of Q^2 the quantity

$$M_{\text{eff}} = \cancel{E}_T + \sum_{\text{jets } j} p_{Tj}.$$

For large M_{eff} the Standard Model background is typically 10% of the signal.



Catania 18

Figure 1: Plot of 5σ reach in jets + \cancel{E}_T channel for mSUGRA model [4, 9].

The reach is thus limited mainly by the \tilde{g} and \tilde{q} production cross sections and hence masses. This reach is shown for the minimal SUGRA model in Fig. 1. Note that the sensitivity for one month at 10% of design luminosity is about 1500 GeV. Of course it will take more than one month to understand the detectors, but nevertheless one might hope for an interesting talk at SUSY08. Squark and gluino decays typically involve one or more intermediate charginos or neutralinos, giving rise to multi-lepton signatures as well as ones involving jets. The reach for such signatures is shown in Figure 2.

The emergence of the SUSY signal from the Standard Model background is illustrated for a typical case in Figure 3. Also shown is the correlation between the peak of the M_{eff} distribution and

$$M_{\text{SUSY}} \equiv \frac{\sum_i M_i \sigma_i}{\sum_i \sigma_i}, \quad M_{\text{SUSY}}^{\text{eff}} \equiv M_{\text{SUSY}} - \frac{M^2(\tilde{\chi}_1^0)}{M_{\text{SUSY}}}$$

Obviously, however, any such inclusive correlation is model dependent.

While the reach plots in Figure 1 apply only to mSUGRA, similar reach in gluino and squark masses should apply to any model in which they decay into an invisible and

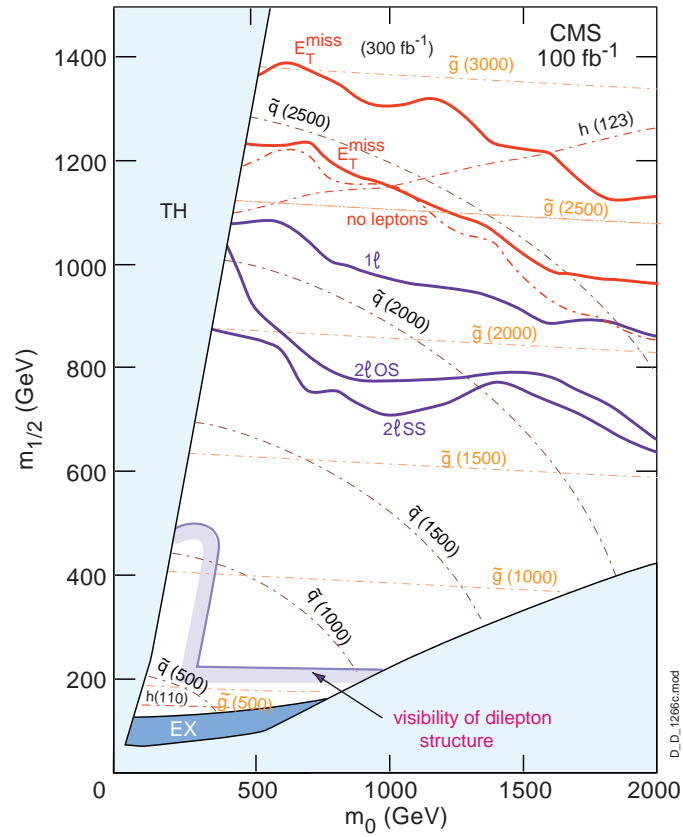


Figure 2: Reach limits in various channels for 100 fb^{-1} [4].

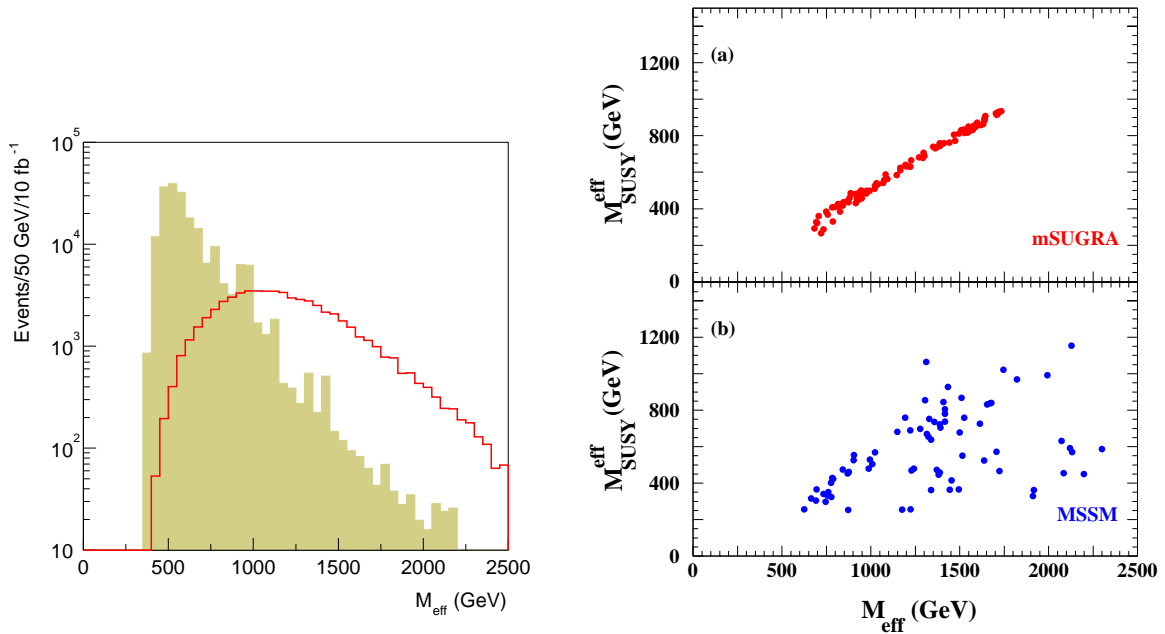


Figure 3: Left: Typical M_{eff} distribution. Right: Correlation of M_{eff} with SUSY mass scale [10].

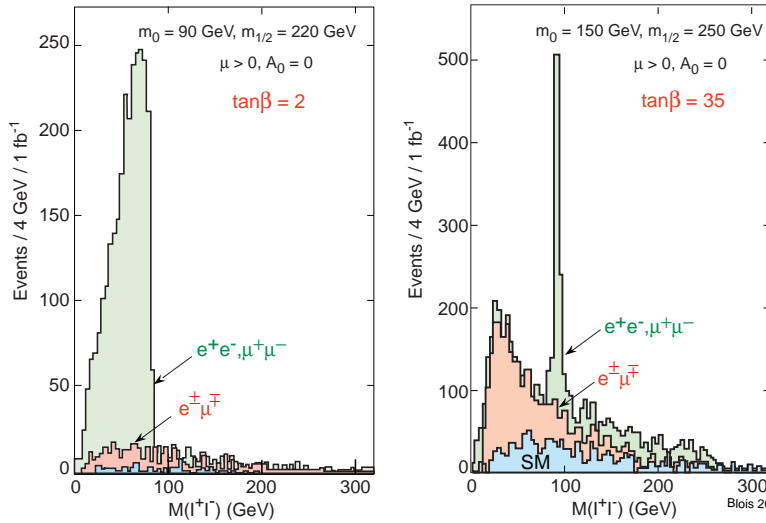


Figure 4: Plot of e^+e^- , $\mu^+\mu^-$ and $e^\pm\mu^\mp$ mass distributions for mSUGRA with 2-body cascade decay (left) and Z plus 3-body decay (right) [12].

relatively light $\tilde{\chi}_1^0$. Some models are easier. For example, GMSB models with prompt $\tilde{\chi}_1^0 \rightarrow \tilde{G}\gamma$ or $\tilde{\ell} \rightarrow \tilde{G}\ell$ decays provide additional photon or lepton handles to suppress Standard Model backgrounds. GMSB models with a quasi-stable $\tilde{\ell}$ provide a penetrating charged particle with $\beta < 1$ that is well measured by the muon detectors. AMSB models give few single leptons but larger \cancel{E}_T . If R parity is violated via $\tilde{\chi}_1^0 \rightarrow \ell^+\ell^-\nu$ or $q\bar{q}\ell, q\bar{q}\nu$, there are again additional leptons. Perhaps the most difficult case is R -violation via $\tilde{\chi}_1^0 \rightarrow cds$, giving multiple jets but no b jets. The background is poorly known, but it seems likely that one must rely on leptonic cascade decays. In general, however, discovery of gluinos and squarks with masses of order 1 TeV appears straightforward. Masses of 3 TeV are of course much more difficult and would probably need a luminosity upgrade.

3 SUSY Measurements using Leptons

If R parity is conserved, then the $\tilde{\chi}_1^0$ is invisible and there are no mass peaks. Nevertheless, kinematic endpoints allow one to determine mass combinations. The simplest example is the decay

For the dilepton signature, events are selected to have two leptons with (typically) $p_{T,\ell} > 10$ GeV and $|\eta_\ell| < 2.5$ in addition to multiple hard jets and large \cancel{E}_T . Then the dominant Standard Model background is $t\bar{t}$. The background from $t\bar{t}$ or from any other Standard Model source involving two independent decays cancels in the combination $e^+e^- + \mu^+\mu^- - e^\pm\mu^\mp$. The same is true for two independent chargino decays in mSUGRA, and it is likely to be true in any SUSY model that avoids $\mu \rightarrow e\gamma$ and other low-energy constraints.

An opposite-sign, same-flavor dilepton signature can arise from a 2-body cascade decay $\tilde{\chi}_2^0 \rightarrow \tilde{\ell}^\pm\ell^\mp \rightarrow \tilde{\chi}_1^0\ell^+\ell^-$, from a 3-body $\tilde{\chi}_2^0 \rightarrow \tilde{\chi}_1^0\ell^+\ell^-$ decay, or from a decay via a Z . All three cases are illustrated in Figure 4. They are clearly distinguished by shape. Such endpoints are observable over a significant fraction of the mSUGRA parameter space, as

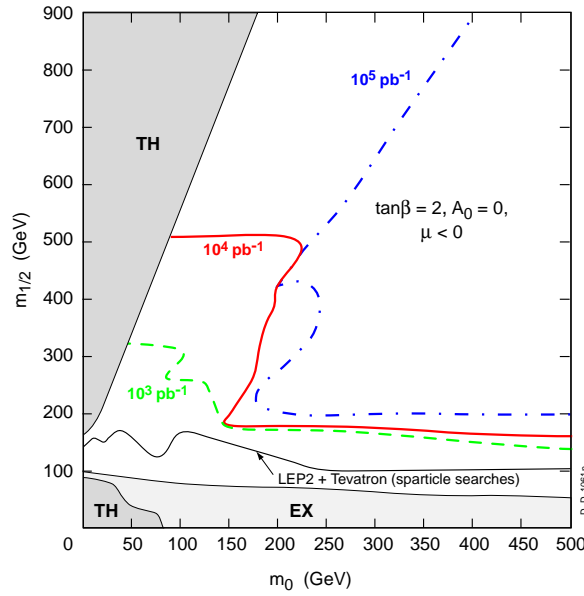


Figure 5: Reach for observing dilepton endpoints in SUGRA models with 1 fb^{-1} , 10 fb^{-1} and 100 fb^{-1} . Theory (TH) and experimental constraints are also indicated [4].

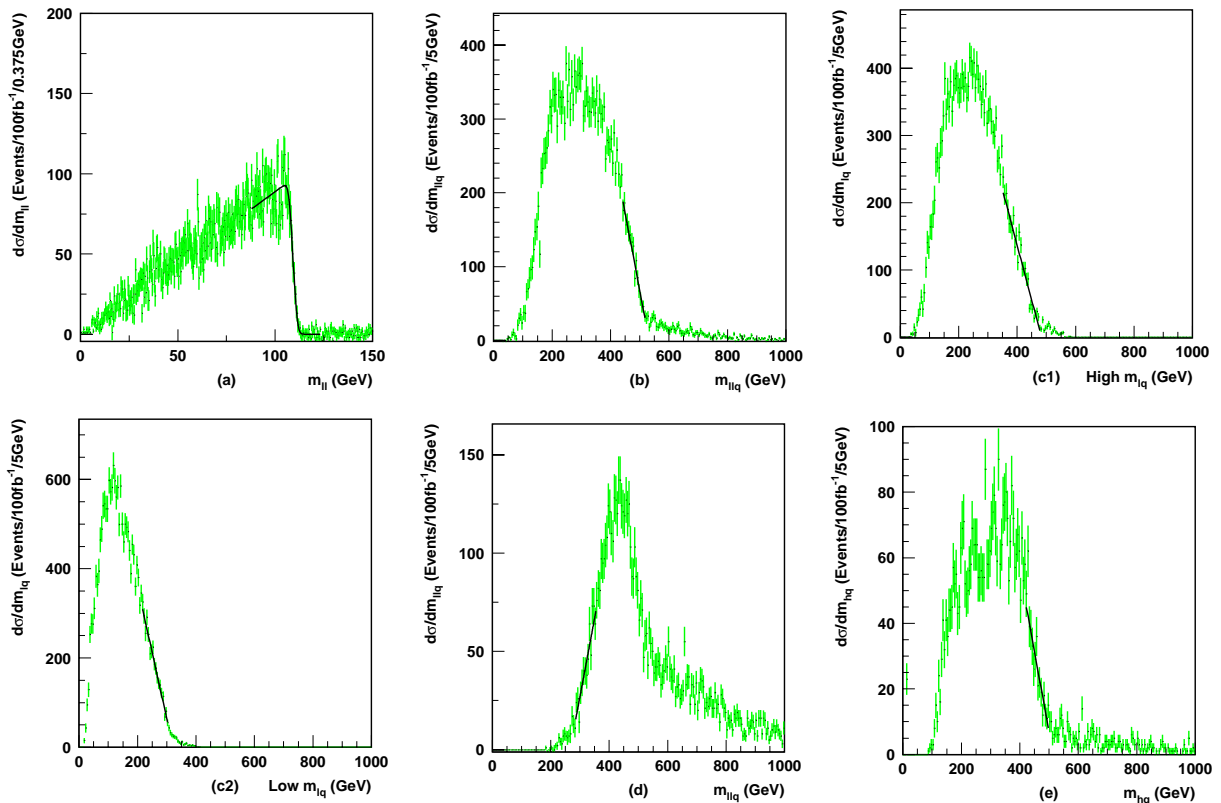


Figure 6: Dilepton + jet distributions for mSUGRA Point 5 as described in the text.

illustrated in Figure 5. In particular, a large part of the mSUGRA parameter space with acceptable cold dark matter has light sleptons and hence enhanced $\ell^+\ell^-$ decays.

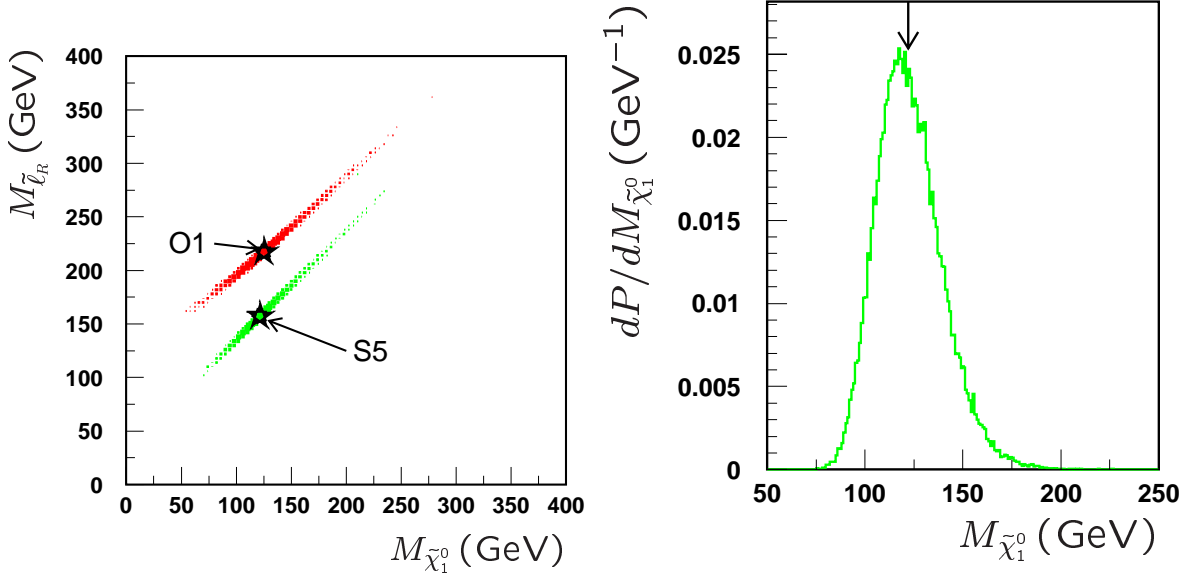


Figure 7: Left: Scatter plot of reconstructed values of $m_\ell \equiv M_{\tilde{\ell}_R}$ vs. $m_1 \equiv M_{\tilde{\chi}_1^0}$ for LHC Point 5 (S5) and for an “optimized string model” (O1) using multiple measurements from the decay chain $\tilde{q}_L \rightarrow \tilde{\chi}_2^0 q \rightarrow \tilde{\ell}_R^\pm \ell^\mp q \rightarrow \tilde{\chi}_1^0 \ell^+ \ell^- q$. The stars mark the input values. Right: Projection onto $M_{\tilde{\chi}_1^0}$ axis [14].

When a longer decay chain can be identified, more combinations of masses can be measured. For example, at mSUGRA Point 5, the dominant source of dileptons is $\tilde{q}_L \rightarrow \tilde{\chi}_2^0 q \rightarrow \tilde{\ell}_R^\pm \ell^\mp q \rightarrow \tilde{\chi}_1^0 \ell^+ \ell^- q$. The gluino is heavier than the squarks, and the hardest jets generally come from the squarks. In such a case, one can form an $\ell^+ \ell^- q$ endpoint and two $\ell^\pm q$ endpoints in addition to the $\ell^+ \ell^-$ one [3, 13]. In addition, if a lower limit on the $\ell^+ \ell^-$ mass is imposed, there is also an $\ell^+ \ell^- q$ threshold.

All of these distributions after experimental selections are shown in Figure 6. The endpoints and thresholds can all be expressed in terms of the masses involved using elementary kinematics, and they provide enough constraints to determine the masses. The results taking estimated errors into account for the $\tilde{\chi}_1^0$ and $\tilde{\ell}_R$ masses are shown in Figure 7 for two models with similar masses. All the masses involved are determined quite accurately as functions of $M_{\tilde{\chi}_1^0}$; in particular the two models can be easily distinguished. The $\tilde{\chi}_1^0$ mass is determined to about 10% through its effect on the kinematics even though it is invisible.

An alternative approach is to reconstruct $\tilde{\chi}_2^0$ momentum assuming that the $\tilde{\chi}_1^0$ mass is known and using

$$\vec{p}_{\tilde{\chi}_2^0} = \vec{p}_{\ell\ell} \left(1 + \frac{M_{\tilde{\chi}_1^0}}{M_{\ell\ell}} \right)$$

While this is exact only for a 3-body $\tilde{\chi}_2^0 \rightarrow \tilde{\chi}_1^0 \ell\ell$ at the endpoint, it can be used as an approximation elsewhere. An analysis for SUGRA Point B ($m_0 = 100$ GeV, $m_{1/2} = 250$ GeV, $A_0 = 0$, $\tan\beta = 10$, $\mu > 0$) using this method looks for $\tilde{g} \rightarrow \tilde{b}\tilde{b} \rightarrow \tilde{\chi}_2^0 b\tilde{b} \rightarrow \tilde{\ell}b\tilde{b} \rightarrow \tilde{\chi}_1^0 \ell b\tilde{b}$. The dilepton distribution after cuts and the reconstructed $\tilde{\chi}_2^0 b$ distribution using $75 < M_{\ell\ell} < 92$ GeV are shown in Figure 8. A second b can be added to reconstruct the gluino mass; see Ref. 15.

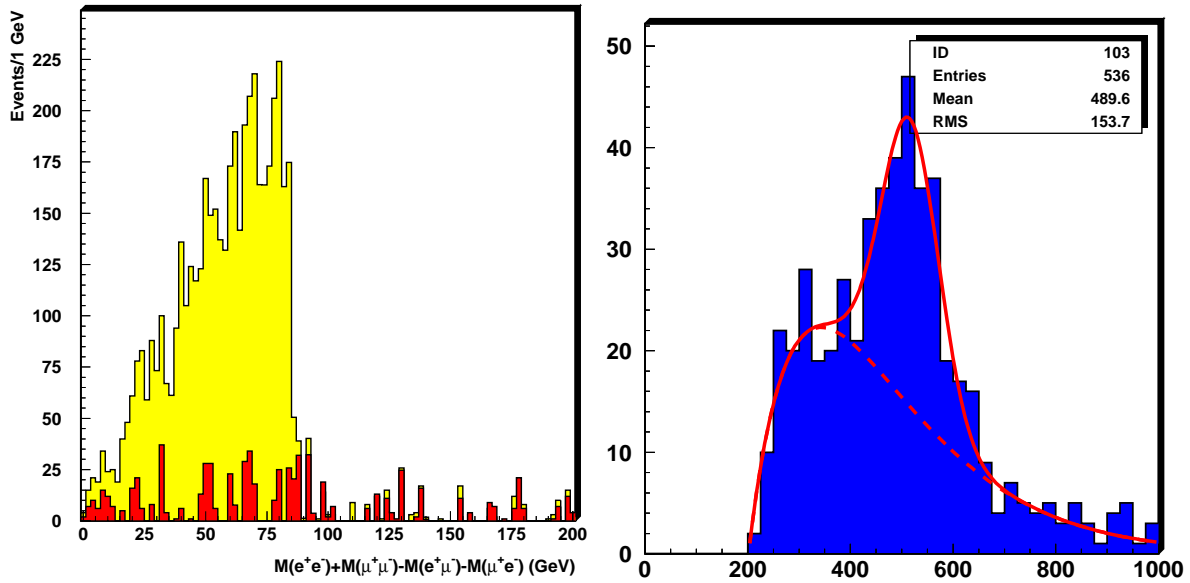


Figure 8: Left: Dilepton distribution for Point B analysis. Right: $M(\tilde{\chi}_2^0 b)$ distribution using inferred $\tilde{\chi}_2^0$ momentum[15].

4 SUSY Measurements using $h \rightarrow b\bar{b}$

If the decay $\tilde{\chi}_2^0 \rightarrow \tilde{\chi}_1^0 h$ is kinematically allowed, it often has a substantial branching ratio. The decay $h \rightarrow b\bar{b}$ can be reconstructed by selecting events with multiple jets plus large \cancel{E}_T and plotting the mass of pairs of jets tagged as b 's. The reach for this signature in mSUGRA, shown in Figure 9, covers a substantial fraction of parameter space. It might well be the discovery mode for the light SUSY Higgs.

If $h \rightarrow b\bar{b}$ can be reconstructed, it can then be combined with jets to determine other masses. In Figure 10 for example, the h was combined with each of the two hardest jets in the event; the smaller of these masses should be less than the $\tilde{q} \rightarrow \tilde{\chi}_1^0 h q$ endpoint. This measurement is less precise than those involving leptons, but it may be useful if the leptonic branching ratios are small.

5 Complex SUSY Signatures

SUSY events can be much more complex than those for the cases discussed above. An example is the “focus point” region: in mSUGRA as m_0 becomes large for fixed values of the other parameters, $\mu \rightarrow 0$ and radiative electroweak symmetry breaking fails. Near this boundary, the $\tilde{\chi}_1^0$ is dominantly Higgsino, leading to acceptable values of cold dark matter [17]. The exact location of the focus point region is very sensitive to details of the SUSY spectrum calculation [18], but such a region surely exists.

In one calculation [19] the mSUGRA point $m_0 = 1500$ GeV, $m_{1/2} = 300$ GeV, $A_0 = 0$, $\tan\beta = 10$, $\mu > 0$ is close to the $\mu = 0$ focus point boundary. Since the squarks are heavy, SUSY production is dominated by $\tilde{g}\tilde{g}$ pairs. The largest \tilde{g} branching ratios are calculated [7] to be $B(\tilde{g} \rightarrow \tilde{\chi}_1^- t\bar{b} + \text{h.c.}) \approx B(\tilde{g} \rightarrow \tilde{\chi}_2^- t\bar{b} + \text{h.c.}) \approx 23\%$. These decays give

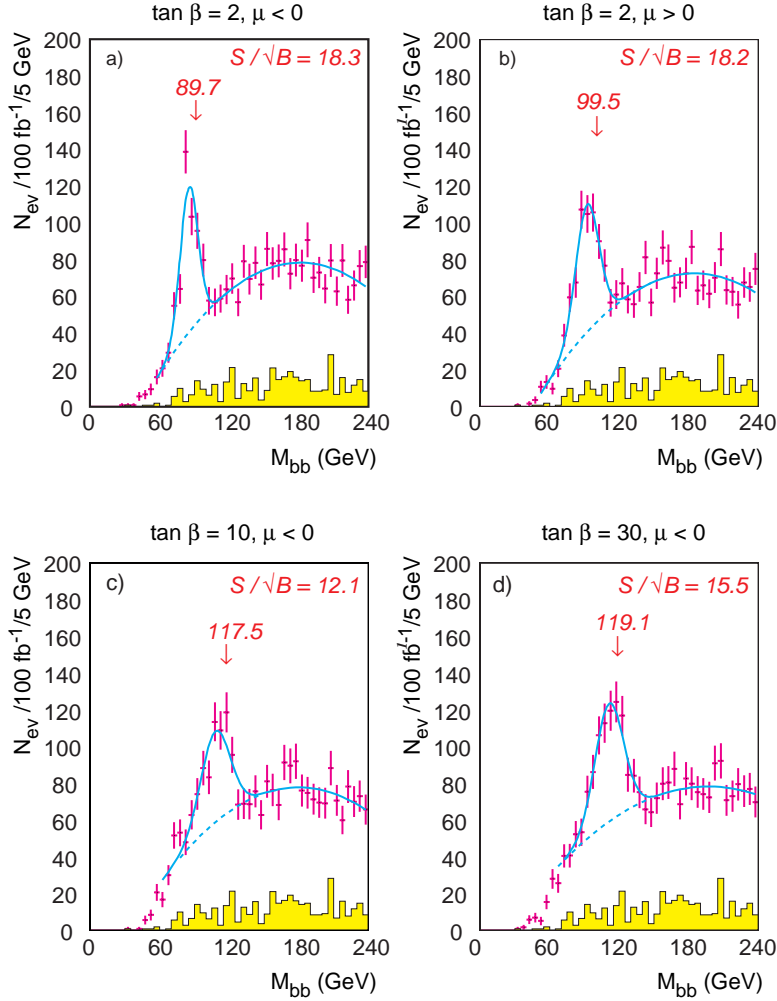


Figure 9: Plot of $b\bar{b}$ dijet mass distribution (points) with $h \rightarrow b\bar{b}$ signal (solid), SUSY background (dashed), and Standard Model background (shaded) for various $\tan\beta$ [16, 4].

events with 12–16 jets and leptons! The methods described previously suffice to find such signals. Many of the basic starting points discussed previously also work; see for example Figure 11. But sorting out the combinatorial background in such complex events is quite difficult and has not yet been solved.

R -parity violation with $\tilde{\chi}_1^0 \rightarrow qq\bar{q}$, and especially $\tilde{\chi}_1^0 \rightarrow cds$ is another example of a SUSY model with very complex signatures. In such models the signal has very high jet multiplicity — nominally six jets just from the $\tilde{\chi}_1^0$ decays — few or no b jets that might be used to reduce the combinatorial background, and small \cancel{E}_T . The QCD background for such events is not well known; the 1-loop QCD corrections to the production of 6-10 jets seem unlikely to be calculated even by the end of LHC running. Estimates based on QCD shower Monte Carlo programs suggest that the backgrounds are comparable to the signals, but this is at best a rough estimate.

For such scenarios, therefore, it is probably necessary to rely on SUSY cascade decays, e.g., $\tilde{\chi}_2^0 \rightarrow \tilde{\ell}^\pm \ell^\mp \rightarrow \tilde{\chi}_1^0 \ell^+ \ell^- \rightarrow qq\bar{q} \ell^+ \ell^-$, to provide additional handles to suppress the QCD

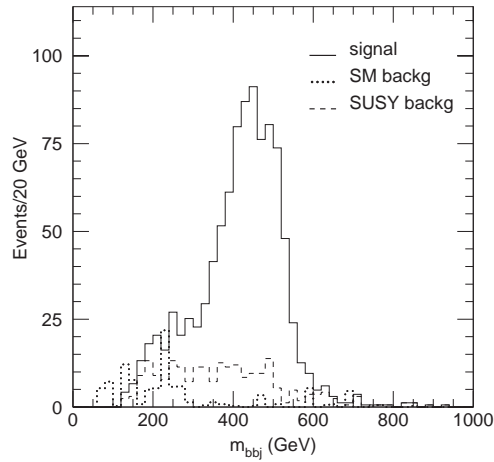


Figure 10: Minimum $M(hj)$ mass from $h \rightarrow b\bar{b}$ combined with two hardest jets [3].

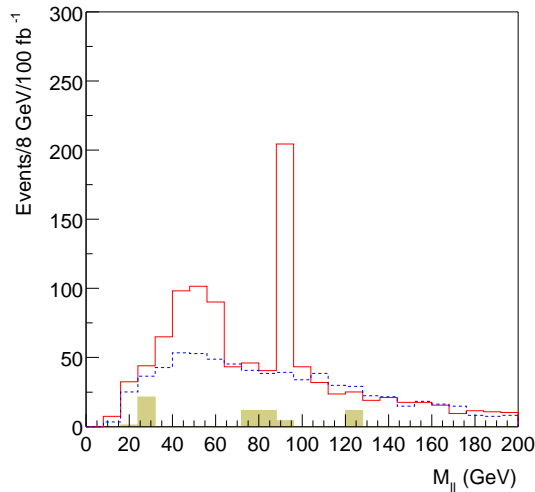


Figure 11: Dilepton mass spectrum for focus point SUSY model[20, 21].

background. One example that has been studied uses such decays with branching ratios taken from mSUGRA Point 5. Even though there are no missing particles, reconstruction is difficult because the jets from the $\tilde{\chi}_1^0$ are soft and the mass resolution is only $\sim 10\%$. Define the mass combinations $M^\pm = M(qqq\ell^+\ell^-) \pm M(qqq)$; then the jet resolution largely cancels for M^- , as can be seen in Figure 12. The distributions in Figure 13 show reasonable distributions in these variables.

These are just two examples of SUSY scenarios giving complex signatures. Such scenarios are certainly possible, and much more work is needed to develop analysis strategies to deal with them.

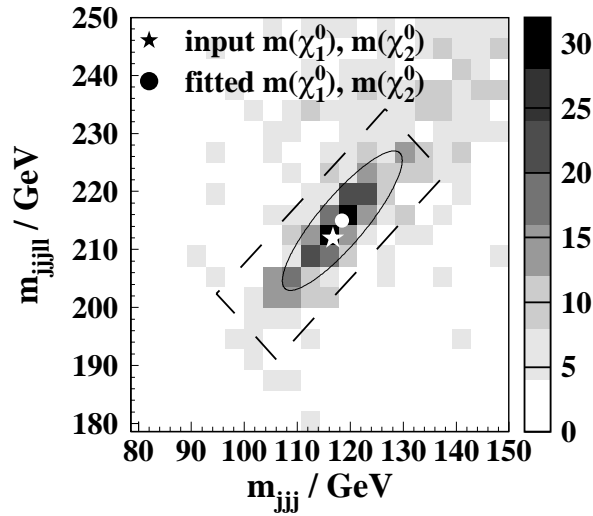


Figure 12: Scatter plot of M^+ vs. M^- for R -violating $\tilde{\chi}_1^0 \rightarrow qq\bar{q}$ decays[22].

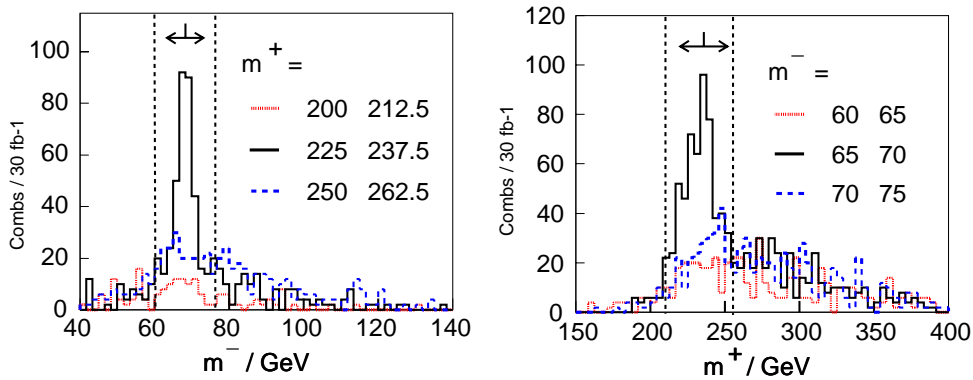


Figure 13: Distributions of $m^{\pm} = M(\ell^+\ell^-qq) \pm M(qqq)$ in R -parity violating SUSY events with $\tilde{\chi}_1^0 \rightarrow qq\bar{q}$ after selecting either the peak or sidebands in m^{\mp} [22].

6 SUSY Signatures with τ 's

The initial motivation for studying τ signatures came from the fact that for large regions of mSUGRA parameter space with $\tan\beta \gg 1$ the only two-body decay modes are $\tilde{\chi}_2^0 \rightarrow \tilde{\tau}_1\tau$ and $\tilde{\chi}_1^{\pm} \rightarrow \tilde{\tau}_1^{\pm}\nu_{\tau}$. Then these modes have branching ratios close to 100%, and all SUSY decays involve τ 's. Such scenarios are disfavored because they tend to give contributions to $g_{\mu} - 2$ much larger than observed.

Low-energy tests of the Standard Model seem to require that the first two generations of squarks and sleptons be nearly degenerate. This degeneracy is not understood in general but does occur in mSUGRA. Even in mSUGRA, however, the third generation of squarks and sleptons is split by renormalization group and left-right mixing effects. Thus, study of the third generation is likely to be essential for understanding SUSY.

Because of technical constraints, the ATLAS and CMS vertex detectors do not have sufficient resolution to identify τ decays cleanly. Hence, leptonic τ decays cannot be distinguished from prompt leptons, and τ 's can only be identified using narrow, one-prong

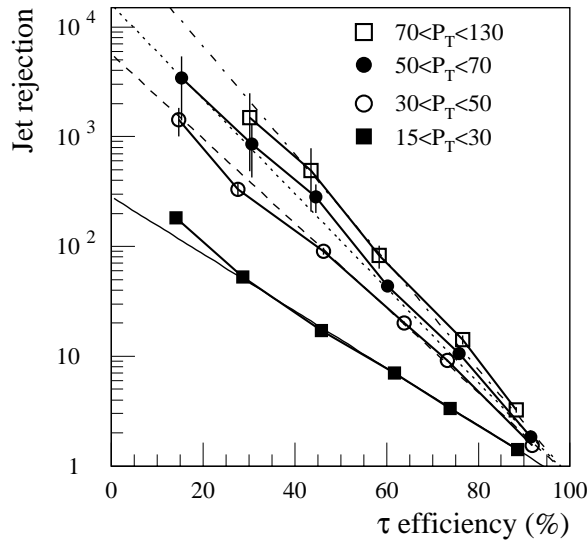


Figure 14: QCD jet rejection vs. efficiency for hadronic τ decays based on full simulation of the ATLAS detector [3].

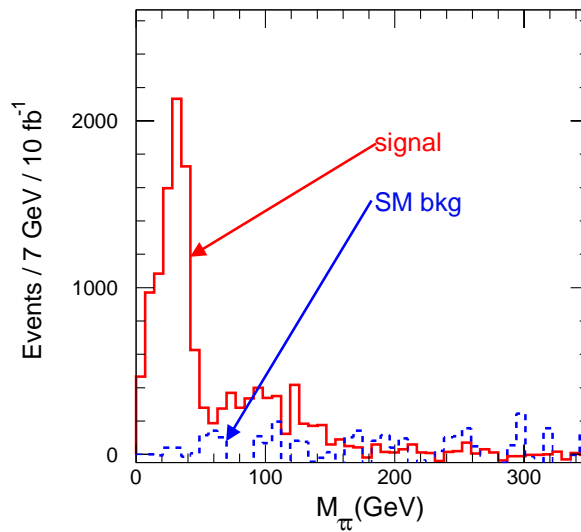


Figure 15: Plot of $\tau^+\tau^- - \tau^+\tau^+$ visible mass distribution with hadronic τ decays at LHC SUGRA Point 6 [3].

jets, for which there is substantial QCD background. As can be seen from Figure 14, the typical jet rejection is a factor of about 100 for a τ efficiency of 50%.

For mSUGRA with $m_0 = m_{1/2} = 200$ GeV, $A_0 = 0$, $\tan\beta = 45$, the only 2-body decays of light gauginos are $\tilde{\chi}_2^0 \rightarrow \tilde{\tau}_1\tau$ and $\tilde{\chi}_1^\pm \rightarrow \tilde{\tau}_1\nu_\tau$. These decays therefore dominate. Since there is \cancel{E}_T both from ν_τ 's and from $\tilde{\chi}_1^0$'s, the τ distributions can only be inferred from their hadronic decay products. Instead of a sharp $\tau\tau$ edge at 59.64 GeV, one would observe the distribution shown in Figure 15.

The visible τ momentum depends both on the momentum and on the polarization of the parent τ . The decay $\tau \rightarrow \pi\nu$ is maximally sensitive to the polarization while high-

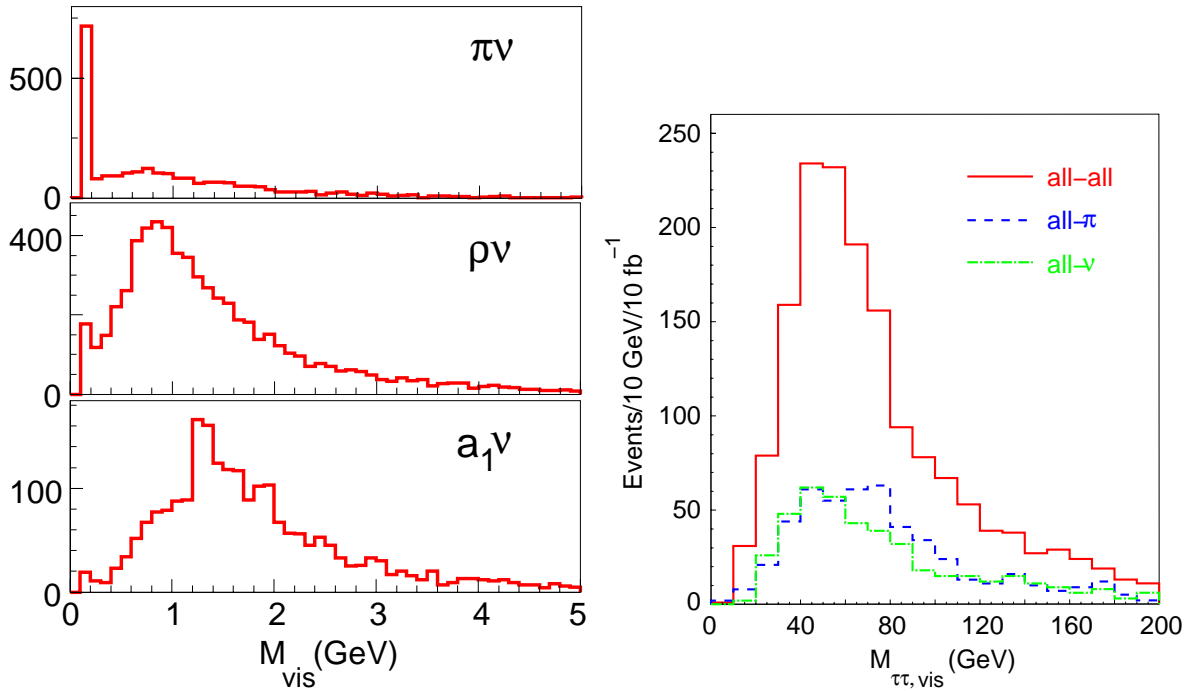


Figure 16: Left: Reconstructed masses for various τ decay modes. Right: $\tau\tau$ mass distribution for all modes, for one $\tau \rightarrow \pi\nu$ decay, and for decays with reversed helicities.

mass decays are rather insensitive to it. A study of the separation of different decay modes has been carried out using a full GEANT-based simulation of τ 's from SUSY events in the ATLAS detector. The visible τ mass is reconstructed by combining charged tracks and electromagnetic calorimeter cells, exploiting the fine granularity of the calorimeter. The reconstructed masses, Figure 16, show a good separation of $\pi\nu$ decays and some difference between $\rho\nu$ and $a_1\nu$ decays. The same figure indicates the sensitivity of the $\tau\tau$ mass distribution to a reversal of helicities.

7 GMSB Signatures

In GMSB models the lightest SUSY particle is the light gravitino \tilde{G} . The phenomenology depends on nature and lifetime of the next lightest particle (NLSP), which can be either the $\tilde{\chi}_1^0$ or a $\tilde{\ell}$. Decays into \tilde{G} lead to more distinctive events and to longer decay chains, such as $\tilde{\chi}_2^0 \rightarrow \tilde{\ell}^\pm \ell^\mp \rightarrow \tilde{\chi}_1^0 \ell^+ \ell^- \rightarrow \tilde{G} \gamma \ell^+ \ell^-$, that can be used to determine SUSY masses [3].

The lifetime for the NLSP to decay to a \tilde{G} is unknown and is an important parameter of the model. Short $\tilde{\chi}_1^0 \rightarrow \tilde{G} \gamma$ lifetimes can be measured by selecting Dalitz decays and using the vertex detector. For $c\tau_{\tilde{\chi}_1^0} \gg 1$ m the signature is occasional photons that do not point to the primary vertex. The ATLAS electromagnetic calorimeter was designed to measure photon angles with $\Delta\theta \approx \frac{60 \text{ m}}{\sqrt{E}}$ to improve the $h \rightarrow \gamma\gamma$ mass resolution. It also has good time resolution, $\Delta t \approx 100$ ps. Both can be exploited to detect long-lived $\tilde{\chi}_1^0 \rightarrow \tilde{G} \gamma$ decays with good efficiency, as seen in Figure 20-65. If no signal is seen, an upper limit of order $c\tau \sim 100$ km could be established [3].

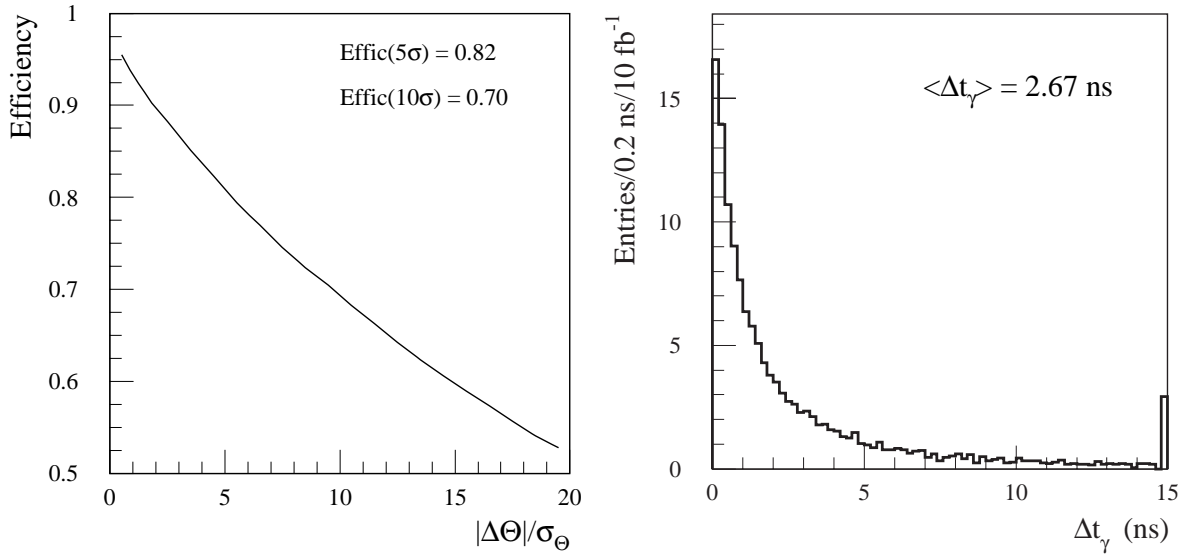


Figure 17: Angle (left) and time delay (right) for photons from long-lived $\tilde{\chi}_1^0 \rightarrow \tilde{G}\gamma$ in the ATLAS detector[3].

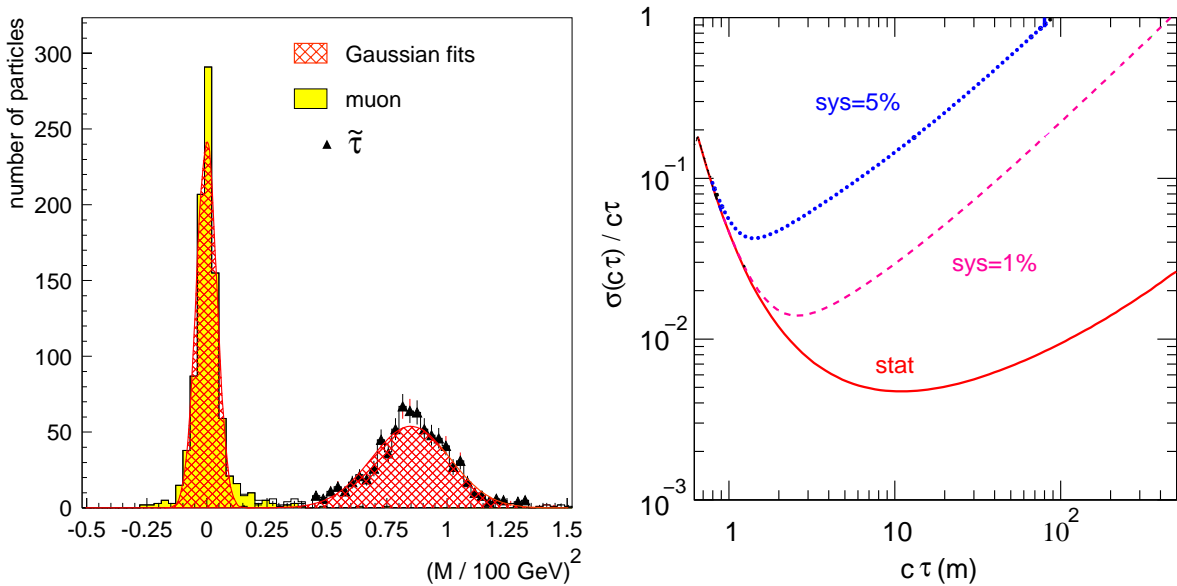


Figure 18: Left: Time of flight separation of muons and quasi-stable $\tilde{\ell}$ [23]. Right: Measurement of $\tilde{\ell}$ lifetime for different estimates of the systematic error on the acceptance [24].

A long-lived slepton NLSP would give tracks with $\beta < 1$ through the calorimeter and muon system. These can be well identified by using the muon system as a time of flight system, as can be seen in Figure 18 [3, 23]. The lifetime can be estimated by counting the number of events with zero, one, and two such tracks, as is also shown in Figure 18. It should also be possible to determine the lifetime by looking for kinks in the central tracker, but developing the needed pattern recognition algorithm is non-trivial and has not yet been attempted.

8 Outlook

If SUSY exists with masses below about 1 TeV, it seems likely that the ATLAS and CMS detectors should find evidence for it shortly after the LHC begins operation. Only a limited number of SUSY models and cases have been investigated so far, and in all cases the answer has been known. These studies seem sufficient, however, to sketch the broad outlines of an initial program of SUSY measurements (assuming that R parity is conserved):

1. Search for an excess of multijet + \cancel{E}_T events over Standard Model predictions, which of course must be checked against other measurements.
2. If such an excess is found, select a sample of SUSY with simple cuts such as those described above.
3. Look for special features such as γ 's or long-lived $\tilde{\ell}$'s in these events.
4. Look for ℓ^\pm , $\ell^+\ell^-$, $\ell^\pm\ell^\pm$, b jets, hadronic τ decays, etc.
5. Try simple endpoint-type analyses such as those described above.

This program looks quite feasible.

There is of course much more information available, including cross sections, branching ratios, and other kinematic distributions. Ultimately one will want to use the first measurements to guide further analyses incorporating all the information. This program will need the full power of the LHC and its detectors.

References

- [1] Atlas Technical proposal, CERN/LHCC/94-43.
- [2] CMS Technical proposal, CERN/LHCC/94-38.
- [3] ATLAS Collaboration, *ATLAS Detector and Physics Performance Technical Design Report*, CERN/LHCC/99-14, <http://atlasinfo.cern.ch/Atlas/GROUPS/PHYSICS/TDR/access.html>.
- [4] S. Abdullin *et al.* [CMS Collaboration], "Discovery potential for supersymmetry in CMS," hep-ph/9806366.
- [5] I. Hinchliffe, F. E. Paige, M. D. Shapiro, J. Soderqvist, and W. Yao, Phys. Rev. D **55**, 5520 (1997) [hep-ph/9610544].
- [6] G. Corcella *et al.*, arXiv: hep-ph/0201201.
- [7] H. Baer, F. E. Paige, S. D. Protopopescu, and X. Tata, "e- reactions," arXiv: hep-ph/0001086.
- [8] T. Sjostrand, L. Lonnblad, and S. Mrenna, arXiv: hep-ph/0108264.

-
- [9] D. Denegri, private communication.
- [10] D. R. Tovey, Phys. Lett. B **498**, 1 (2001) [arXiv: hep-ph/0006276].
- [11] F. Gianotti, et al., hep-ph/0204087.
- [12] D. Denegri, W. Majerotto, and L. Rurura, Phys. Rev. **D60** (1999), 035008;
L. Rurua, PhD Thesis, Institute of High Energy Physics, Austrian Academy of Sciences, 1999.
- [13] H. Bachacou, I. Hinchliffe, and F. E. Paige, Phys. Rev. D **62**, 015009 (2000) [hep-ph/9907518].
- [14] B. C. Allanach, C. G. Lester, M. A. Parker, and B. R. Webber, at the L! JHEP**0009**, 004 (2000) [hep-ph/0007009].
- [15] Alessia Tricomi, these proceedings.
- [16] S. Abdullin, CMS Note 1997/070.
- [17] J. L. Feng, K. T. Matchev, and F. Wilczek, Phys. Lett. B **482**, 388 (2000) [arXiv: hep-ph/0004043].
- [18] B. Allanach, S. Kraml, and W. Porod, arXiv: hep-ph/0207314.
- [19] M. Battaglia *et al.*, in *Proc. of the APS/DPF/DPB Summer Study on the Future of Particle Physics (Snowmass 2001)* ed. N. Graf, arXiv: hep-ph/0112013.
- [20] I. Hinchliffe and F. E. Paige, in *Proc. of the APS/DPF/DPB Summer Study on the Future of Particle Physics (Snowmass 2001)* ed. N. Graf, SNOWMASS-2001-E401 Prepared for APS / DPF / DPB Summer Study on the Future of Particle Physics (Snowmass 2001), Snowmass, Colorado, 30 Jun - 21 Jul 2001.
- [21] I. Hinchliffe and F. E. Paige, in *Proc. of the APS/DPF/DPB Summer Study on the Future of Particle Physics (Snowmass 2001)* ed. N. Graf, SNOWMASS-2001-E402 Prepared for APS / DPF / DPB Summer Study on the Future of Particle Physics (Snowmass 2001), Snowmass, Colorado, 30 Jun - 21 Jul 2001.
- [22] B. C. Allanach, A. J. Barr, L. Drage, C. G. Lester, D. Morgan, M. A. Parker, P. Richardson, and B. R. Webber, arXiv: hep-ph/0102173.
- [23] M. Kazana, G. Wrochna, and P. Zalewski, CMS CR 1999/019 (June, 1999).
- [24] S. Ambrosanio, B. Mele, A. Nisati, S. Petrarca, G. Polesello, A. Rimoldi, and G. Salvini, arXiv: hep-ph/0012192.